The effect of temperature on bubble lattice formation in copper under *in situ* He ion irradiation

Aidan M Robinson [a,*], Philip D Edmondson [a,**], Colin English [b], Sergio Lozano-Perez [a], Graeme Greaves [c], Jonathan A Hinks [c], Stephen E Donnelly [c], and Chris R M Grovenor [a]

[a] *University of Oxford, Department of Materials, Parks Road, Oxford, OX1 3PH, UK*

[b] *NNL, Culham Science Centre, Abingdon, Oxfordshire, OX14 3DB*

[c] *School of Computing and Engineering, University of Huddersfield, HD1 3DH, UK*

Abstract:

In situ ion irradiation in a transmission electron microscope was used to investigate the effects of temperature on radiation-induced bubble lattice formation in Cu by low energy (12 keV) helium ions. Bubble lattices were observed to form between –100 and 100°C, but at 200°C lattice formation was impeded by continued growth and agglomeration of bubbles. Both nucleation of bubbles, and to a lesser extent bubble lattice formation, are observed at lower fluences as temperature increases, which we suggest is due to increased point defect mobility. Previous work on point defect concentrations in irradiated copper is considered when interpreting these results.

Keywords: Bubble lattice, self-interstitial atoms, *in situ* ion irradiation, copper

* Corresponding author: Aidan Robinson (aidan.robinson@materials.ox.ac.uk)
** Current address: Materials Science & Technology Division, Oak Ridge National Laboratory, Oak Ridge, TN 38731, USA

The inert gases He, Kr and Xe are all by-products of nuclear reactions; He from (n, α) and fission reactions, while Kr and Xe are fission products formed during the burning of nuclear fuels. These gases are generally insoluble in metal and ceramic materials and therefore precipitate out into pressurised gas bubbles in the materials used in reactor cores. These bubbles are of considerable interest to the nuclear materials community as their presence can encourage both creep damage and swelling as well as causing life-limiting embrittlement of structural materials exposed to these extreme environments [1]. Voids can also be created by agglomeration of radiation-induced vacancies, and can have similar deleterious effects on mechanical properties.

A random distribution of bubbles may contribute significantly to creep and mechanical property degradation of reactor components, but when these bubbles are arranged in an ordered lattice these damaging effects may be reduced [2]. Bubble lattices are known to form in materials under the non-equilibrium conditions found in modern nuclear reactor cores [3], and gas accumulation within a material is known to cause dimensional changes and induce embrittlement to the component [4]. Bubble lattices have thus been investigated in order to better understand both their formation mechanisms and to further understand degradation expected in in-service core reactor components.

The first evidence for periodic ordering of radiation induced cavities was reported by Evans in molybdenum irradiated with 2 MeV nitrogen ions [5] where a body-centred cubic (bcc) ordered array of voids was found to replicate the lattice of the host metal, with a lattice parameter two orders of magnitude larger. Since then, numerous *ex situ* irradiation experiments have yielded samples exhibiting a 3-dimensional void lattice as defined by diffraction analysis [6,7].

Bubble lattices are characterised by having long range ordering on low-index crystallographic planes [8] and have been shown to form in face-centred cubic (fcc) as well as in bcc materials [5,9–11]. One notable exception to the general rule that a bubble lattice has the same structure as the matrix material is bcc U-7Mo fuel particles embedded in an Al-alloy matrix, in which an fcc fission gas bubble lattice structure was reported rather than the bcc structure of the host lattice [12]. Bubble lattices that form in hcp materials are generally found to show ordering only parallel to the basal plane [13].

One proposed mechanism for the formation of bubble lattices is that it is driven by elastic interactions between bubbles [14], but Willis argued that the long range ordering synonymous with a bubble lattice is found over distances much larger than the effect of the anisotropy of elastic constants [15]. Hence the short range elastic interactions between bubbles are unlikely to be solely responsible for bubble lattice formation. The mechanism of isomorphic decomposition [16] was also ruled out as it does not take into account the non-equilibrium conditions found during irradiation [17].

As a means of relieving stress, over-pressurised bubbles have been found to 'punch-out' self-interstitial atoms (SIAs) and/or interstitial dislocation loops in the direction of the glide plane, resulting in bubble movement and alignment along the glide cylinders [18,19]. As a possible mechanism for bubble ordering, however, this was discredited as bubbles would move away from, not towards, the ordering direction[17]. Also, it is uncertain whether the bubble pressure is sufficiently high to induce loop punching at the fluence levels under which bubble lattices are found in ion implantation experiments, $\sim 10^{16}$–10^{17} ions/cm^{-2} [17]. Voids do not become pressurised and hence cannot punch out interstitials or dislocations, therefore this hypothesised mechanism could not explain the existence of void lattices.

Currently, there is a general consensus that a mechanism involving the anisotropic diffusion of host metal SIAs is most likely to explain bubble lattice formation [20,21]. Such a mechanism was initially put forward by Evans [8], who later modelled bubble lattice formation using rate theory computer simulations of 2D interstitial diffusion [22]. SIA diffusion occurs predominantly along the close-packed directions of the host matrix, leading to bubble ordering along these directions, and so creates bubble lattice structures that reflect bcc and fcc matrix structures and basal plane alignment in hcp materials. The {111} and the {100} family of planes have the highest packing density for bcc and fcc structures respectively which helps explain the presence of 3 dimensional lattices, while in hcp crystals the single (0001) plane is the most close packed leading to only 1 dimensional ordering.

In recent studies, *in situ* irradiation experiments of bubble lattice formation have been implemented to complement protracted irradiation campaigns in reactors [23] and the ion irradiation of bulk specimens. *In situ* ion irradiation offers the major advantage that the dynamic processes of irradiation can be directly observed as they occur. Samples irradiated *in situ* have been shown to yield results comparable to those obtained during irradiation of bulk specimens [9,24]. Such techniques can be useful in exploring the mechanisms of bubble lattice formation. This paper reports the observation and characterisation of bubble lattices in copper formed under *in situ* irradiation in a transmission electron microscope (TEM).

Samples were prepared from a sheet of oxygen-free high thermal conductivity (OFHC) copper. Disks 0.2mm thick and 3mm in diameter were prepared by mechanical punching directly from the OFHC copper sheet. TEM samples were produced by electropolishing the disks in a Struers TENUPOL™ device with nitric acid (10%) and methanol (90%) electrolyte in a temperature range of –20°C to –5°C using a voltage of 25V. Samples were then further polished using Precision Ion Polishing system (PIPs) to achieve adequate electron transparency. TEM *in situ* ion irradiations with concurrent examination was performed at the MIAMI facility using a modified JEOL JEM-2000FX microscope operated at 200kV interfaced with a low energy ion accelerator [25].

The samples were irradiated *in situ* with 12 keV He ions such that the highest concentration of He ions was implanted into the middle of the thin foil copper samples as predicted by the Stopping and Ranges of Ions in Matter (SRIM) program version 2013 [26]. Full damage cascade SRIM calculations were performed using a material density of 8.92 gm cm^{-3} and a displacement threshold energy, E_d, of 25eV. Results from SRIM calculations were also used to convert the irradiation fluence into displacements per atom (dpa) values into a 100nm thick sample. While the implantation is being carried out, the TEM illumination was defocussed to limit the impact

of any heating by the electron beam and to minimise displacement of He atoms from the bubbles.

When imaging bubbles (or voids) in the TEM it is desirable to tilt the specimen from the exact Bragg condition in order to minimise the diffraction contrast in the image. However to study the formation of bubble lattices, it is preferable for samples to be tilted close to exact down-zone conditions [27] in order to provide the best opportunity to see the alignment of the bubbles during lattice formation (i.e. close to the zone-axis of the bubble lattice). As a result of this limitation some diffraction contrast is inevitable. Due to Fresnel fringes bubbles appear as light or dark spots when viewed at over and under focus respectively.

Implantation of samples was conducted in regular fluence steps, and images recorded after each step. The dose was calculated after implantation based on continuous ion current measurements on a skimming aperture during irradiation, and at the specimen position at the beginning and end of each experiment [25]. Implantation ended when real-time fast Fourier transforms (FFTs) of the sample image displayed a regular cubic super structure (see inset of figure 1b, indicating that the bubbles had aligned into a bubble lattice. At some temperatures it was observed that the bubbles began to agglomerate before any lattice was formed.

Bubble lattices were observed to form in Cu during *in situ* 12 keV He irradiation over a temperature range of –100 to 100°C. A representative area of a sample irradiated at 100°C prior to and after the formation of a bubble lattice is shown in Figure 1. An amorphous and an ordered array of bubbles are clearly evident in Figure 1a and 1b, respectively, and confirmed by the inset FFTs. During irradiation at 200°C bubble lattices did not form, instead the bubbles underwent continuous growth whilst remaining in a random array (Figure 2). A summary of the fluences and damage levels at which bubbles were first observed to nucleate and then to form lattices is given in Table 1, along with the average bubble diameters and the edge-to-edge inter-bubble spacing. From these results there are three main observations of interest; the size (and distribution) of bubbles as a function of temperature, the conditions under which bubble lattices form, and the difference in the change in required dpa and fluence for bubble and bubble lattice formation. A notable observation is that the bubble size distributions under conditions where bubble lattices were formed are very uniform, unlike the size distribution when the bubbles remained in a disordered arrangement. This is evident in the histogram shown in Figure 3. The divergence in the average size for bubbles arranged in lattices was found to be ≤15%, with the bubbles remaining approximately 2nm in diameter. It should be noted that the measurement of bubble sizes when in a lattice is likely to be the combined projected width of a column of bubbles, and as such the actual divergence in sizes may be smaller. The range of bubble diameters at 200°C (at which temperature bubble lattices did not form) was found to be much larger, with a larger average bubble size of ~3nm and a distribution of <25%. Preliminary experiments on the effects of dose rate on the initial formation of bubbles showed bubbles becoming resolvable after comparable times of irradiation with little apparent dependence on the fluence. Samples were irradiated at room temperature with dose rates of 1.1×10^{13} ions/cm^2/s and 8.4×10^{13} ions/cm^2/s, and in both cases bubbles were first observed after 420 seconds. This equates to a fluence of 6.6×10^{13} ions/cm^2 in the low dose sample and 5×10^{14} ions/cm^2 in the high dose sample. This could be a result of variations in thickness in different specimens and the availability of surface sinks at different distances from the implanted damage region or an indication of minimal dose rate dependence on the rate of bubble lattice formation,

however dose rate dependence of irradiation damage structures of different kinds have been reported by several groups [28–30].

The nucleation and growth of He bubbles as a function of ion fluence and substrate temperature occurs through the interaction of implanted He and radiation-induced point defects to create bubble nucleation sites. We observed that bubbles become observable at much total fluence values as the temperature increased, so that temperature rather than the aggregate He ion fluence seems to be a dominant criterion for bubble formation. Our *in situ* observations show that bubbles nucleate and grow at a quicker rate in the 200°C sample, whereas below 200°C bubbles nucleate and grow at a slower rate yet exhibit a much greater level of uniformity in their size distribution.

Our experimental data also shows that, under the irradiation conditions used bubble lattices form in copper at temperatures between -100 and 100°C but are inhibited at 200°C; indicating that above 100°C a mechanism that suppresses lattice formation is activated. In copper there are thought to be five main recovery stages during annealing after irradiation damage. Stage III is attributed to the activation of migration of interstitials and stage IV is where the temperature exceeds the required activation energy for vacancies to become mobile [31]. The temperatures at which we observe bubble lattices to form lie within the temperature range for stage III in this previous work, but once the temperature reaches that characteristic of stage IV bubble lattices does not form. We theorise that the activated mobility of vacancies, and therefore reduction in interstitial defect sinks could explain the inability of a bubble lattice to form at 200°C. A reduced vacancy-interstitial recombination rate is also observed at higher temperatures [15] resulting in a greater abundance of free vacancies. Hence we see the rapid formation of larger bubbles and the preferential growth of few large defects as opposed to uniform bubble growth above 100°C.

Another observation from these experiments is that enhanced bubble growth occurs at grain boundaries during irradiation above 200°C as shown in Figure 4, presumably as a result of a combination of vacancy diffusion in the grain interiors and fast diffusion at grain boundaries. [32,33]. At temperatures where vacancies are mobile they can be captured by grain boundaries and will then diffuse preferentially along the boundary plane. As the number of trapped vacancies increases (along with He atoms that also diffuse through the lattice and become trapped at grain boundaries), they begin to agglomerate here and form bubbles. Migration along the grain boundaries leads to enhanced growth and/or coalescence of existing bubbles leading to the rapid formation of large bubbles. This kind of process could lead to embrittlement and contribute to severe creep deformation.

In conclusion, TEM with *in situ* He ion irradiation has been used to study the thermal dependence of bubble lattice formation in copper. It was observed that at temperatures between –100 and 100°C bubble lattices form, whilst at 200°C bubble lattice formation is inhibited. This is in agreement with previous studies of *ex situ* implantation of He which reported that bubble lattices will form at 0.22 T_m in copper, after approximately 4×10^{21} ions/cm^2 at 30 keV [23,34]. We have demonstrated that - under these irradiation conditions - between 0.27 and 0.35 T_m there is a transition which inhibits the bubble lattice, and have related this observation to previously reported changes in point defect behaviour in irradiated fcc materials.

The authors would like to thank Rolls Royce for their support and funding, and J.H. Evans for his helpful advice. PDE acknowledges funding from the UK's Engineering and Physical Science Research Council (EPSRC) under grant EP/K030043/1. The MIAMI facility was constructed with EPSRC support under grant EP/E017266/1.

References

[1] R. Adamson, Z. Plus, F. Garzarolli, C. Patterson, In-Reactor Creep of Zirconium Alloys Authors, 2009.

[2] V.I. Dubinko, V. V. Slezov, a. V. Tur, V. V. Yanovsky, Radiat. Eff. 100 (1986) 85.

[3] H. van Dam, T. van der Hagen, J. Hoogenboom, Nuclear Reactor Physics, 2005.

[4] A.J.E. Foreman, B.N. Singh, J. Nucl. Mater. 143 (1986) 672.

[5] J. Evans, Nature 229 (1971) 403.

[6] S.L. Sass, B.L. Eyre, Philos. Mag. 27 (1973) 1447.

[7] F.E. Lawson, P.B. Johnson, J. Nucl. Mater. 252 (1998) 34.

[8] J. Evans, J. Nucl. Mater. 119 (1983) 180.

[9] D.J. Mazey, B.L. Eyre, J.H. Evans, J. Nucl. Mater. 64 (1977) 145.

[10] P. Johnson, D. Mazey, J. Nucl. Mater. 91 (1980) 41.

[11] K. Krishan, Radiat. Eff. 66 (1982) 121.

[12] J. Gan, D.D. Keiser, D.M. Wachs, a. B. Robinson, B.D. Miller, T.R. Allen, J. Nucl. Mater. 396 (2010) 234.

[13] J.H. Evans, D.J. Mazey, J. Nucl. Mater. 138 (1986) 16.

[14] K. Malen, R. Bullough, in:, BNES Conf., 1971, p. 1971.

[15] J. Willis, J. Mech. Phys. Solids 23 (1975) 129.

[16] E. Johnson, L.T. Chadderton, Radiat. Eff. 79 (1983) 183.

[17] J.H. Evans, J. Nucl. Mater. 210 (1994) 230.

[18] C.H. Woo, W. Frank, J. Nucl. Mater. 137 (1985) 7.

[19] S.E. Donnelly, Radiat. Eff. 90 (1985) 1.

[20] R. Boothby, J. Hyde, S. Lozano-Perez, S. Donnelly, J. Minshull, Bubble Lattice Formation: Literature Review and Areas of Future Work, 2010.

[21] D. Walgraef, J. Lauzeral, N.M. Ghoniem, Phys. Rev. B 53 (1996) 782.

[22] J.H. Evans, J. Nucl. Mater. 132 (1985) 147.

[23] P.B. Johnson, D.J. Mazey, J.H. Evans, Radiat. Eff. 78 (1983) 147.

[24] P.B. Johnson, F. Lawson, Nucl. Instruments Methods Phys. Res. Sect. B Beam Interact. with Mater. Atoms 243 (2006) 325.

[25] J. a. Hinks, J. a. van den Berg, S.E. Donnelly, J. Vac. Sci. Technol. A Vacuum, Surfaces, Film. 29 (2011) 21003.

[26] J. Ziegler, J. Appl. Phys. 85 (1999) 1249.

[27] L.T. Chadderton, E. Johnson, T. Wohlenberg, Phys. Scr. 13 (1976) 127.

[28] S.X. Wang, L.M. Wang, R.C. Ewing, Phys. Rev. B 63 (2000) 24105.

[29] C.D. Hardie, C. a. Williams, S. Xu, S.G. Roberts, J. Nucl. Mater. 439 (2013) 33.

[30] O.W. Holland, D. Fathy, Radiat. Eff. 90 (1985) 127.

[31] W. Schilling, K. Sonnenberg, J. Phys. F Met. Phys. 3 (2001) 322.

[32] P.D. Edmondson, C.M. Parish, Y. Zhang, a. Hallén, M.K. Miller, Scr. Mater. 65 (2011) 731.

[33] T. Yamamota, O. GR, K. RJ, W. BD, Fusion Reactor Materials Program Semiannular Report 7/1 to 12/31/2010 DOE/ER-0313/49, 2010.

[34] P. Johnson, D. Mazey, J. Nucl. Mater. 94 (1980) 721.

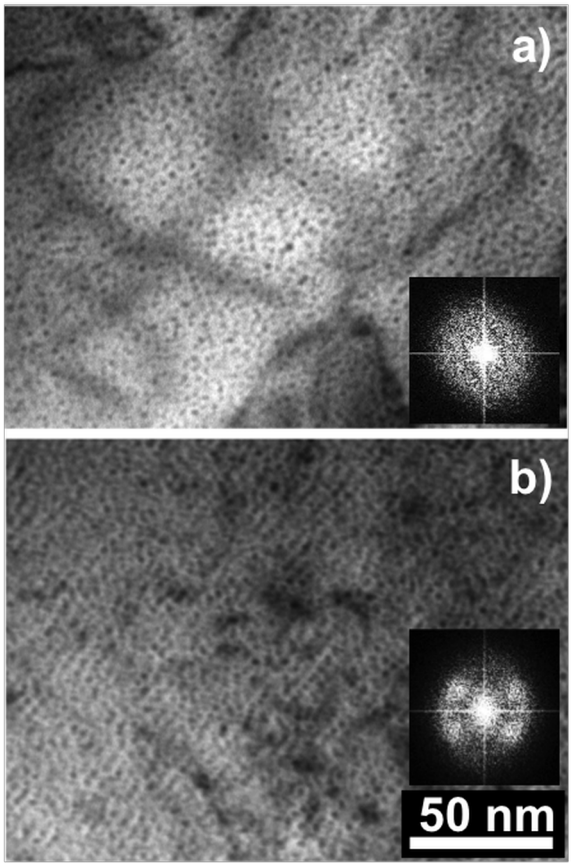

Figure 1: Bubble arrays and inset FFTs from the same sample implanted at 100°C to (a) 3.59 x 10^{16} ions cm^{-2} showing an amorphous bubble array and then (b) at 6.33 x 10^{16} ions cm^{-2} where a lattice has formed. In both figures, the bubbles are observed as dark spots due to the overfocussed imaging condition.

Irradiation temperature (°C)	dpa at which bubbles were observed	Fluence at which bubbles were observed (x 10^{16} ions cm^{-2})	dpa at which bubble lattices were observed	Fluence at which bubble lattices were observed (x 10^{16} ions cm^{-2})	Bubble diameter (nm)	Spacing between bubbles (nm)	Bubble lattice parameter (nm)
-100	2.54	5.9	5.48	12.9	1.8 ± 0.3	1.2 ± 0.3	3.0 ± 0.3
26	0.40	0.94	2.09	4.9	2.1 ± 0.3	1.2 ± 0.3	3.3 ± 0.3
100	0.19	0.45	2.69	6.3	2.4 ± 0.3	1.4 ± 0.3	3.8 ± 0.3
200	0.0045	0.11	N/A	N/A	N/A	N/A	N/A

Table 1. Average bubble size and spacing at the point where a bubble lattice could be detected. dpa values at this point also provided

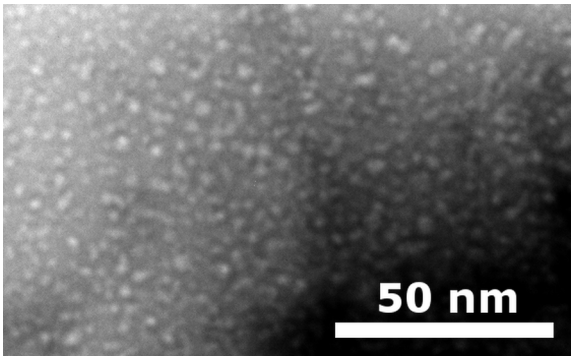

Figure 2: A TEM image from the sample irradiated at 200°C showing the irregular size and shape of the growing bubbles. Bubble lattices were not seen to form during irradiation at this temperature.

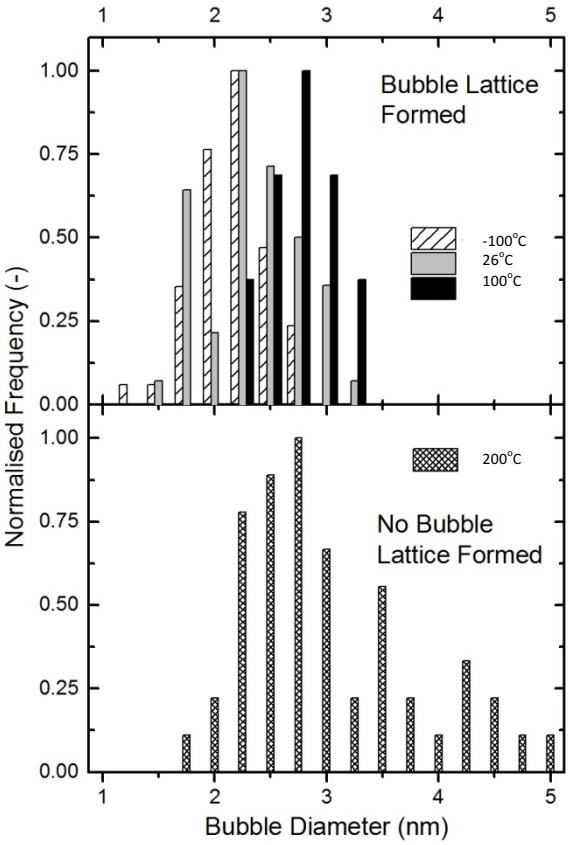

Figure 3. Histograms of the bubble size distributions for the bubbles in a developed lattice (top) and when no lattice was formed (bottom).

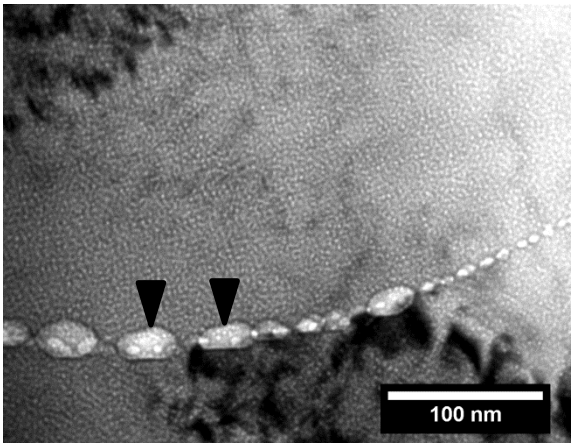

Figure 4: Formation of large bubbles (arrowed) at a grain boundary at 200°C.